AIP | Physics of Fluids

Dynamics of a Janus drop in an external flow

S. Shklyaev, A. O. Ivantsov, M. Díaz-Maldonado, and U. M. Córdova-Figueroa

Citation: Phys. Fluids **25**, 082105 (2013); doi: 10.1063/1.4817541
View online: http://dx.doi.org/10.1063/1.4817541
View Table of Contents: http://pof.aip.org/resource/1/PHFLE6/v25/i8
Published by the AIP Publishing LLC.

PHYSICS OF FLUIDS **25**, 082105 (2013)

Dynamics of a Janus drop in an external flow

S. Shklyaev,[1,2] A. O. Ivantsov,[2] M. Díaz-Maldonado,[1]
and U. M. Córdova-Figueroa[1]
[1]*Department of Chemical Engineering, University of Puerto Rico – Mayagüez, Mayagüez, Puerto Rico 00681, USA*
[2]*Institute of Continuous Media Mechanics, Ural Branch of the Russian Academy of Sciences, Perm 614013, Russia*

(Received 23 June 2013; accepted 21 July 2013; published online 13 August 2013)

The steady motion of a Janus drop under a uniform external flow is considered. First, we analyze the equilibrium shape of a Janus-like drop in a motionless ambient fluid, i.e., the special case of a nearly spherical compound drop with a nearly flat internal interface. This configuration is realizable when the liquids comprising the drop have close interfacial tensions with the ambient fluid, but a small interfacial tension between each other. Then, we consider the flow past a perfect Janus drop composed of two hemispherical domains each occupied by a different fluid. For the sake of simplicity, all the interfaces are assumed nondeformable. The problem is solved both analytically, by means of the Lamb expansion, and numerically. The relation between the flow velocity and the force imposed on the drop, which is a generalization of the classical Hadamard–Rybczynski formula, is found. A torque is also imposed on the drop in the general case. The stable regime of motion of a torque-free drop is found to be axisymmetric, with the less viscous fluid at the upstream face. For this particular configuration, the deformation of the internal interface is also found employing a perturbation technique, whereas the distortion of the drop surface can be safely neglected. © *2013 AIP Publishing LLC*. [http://dx.doi.org/10.1063/1.4817541]

I. INTRODUCTION

The importance and perspectives of Janus particles were predicted by de Gennes in his Nobel lecture[1] more than twenty years ago. Last decade has witnessed a boom in the study of multi-compartmental particles and their simplest representative, a Janus particle. Potential applications of these particles range from useful blocks in the design of modern (smart) materials to sensors or self-propelling particles (motors). For this reason many groups are elaborating the experimental methods of Janus particle synthesis, see the surveys in Refs. 2 and 3.

One of such techniques provides the main application of Janus drops[4–6] being very promising because both particle size and compartment can be precisely controlled. This approach includes a microfluidic generation of a Janus drop usually by means of a two-step method: a sequence of two Y-junctions with opposite wettabilities (e.g., hydrophilic and hydrophobic) of the boundaries. One-step production of Janus drops is discussed in Ref. 7; creation of drops containing three liquids is described in Ref. 8. Usually the liquids comprising the Janus drop contain a dispersed monomer, and further polymerization (by means of heating, ultraviolet radiation, etc.) of the monomer produces a Janus particle.

Another important application of Janus drops is creating amphiphilic particles, e.g., by adsorption of nanoparticles (or polymers, surfactant molecules) of different chemical or physical functionalities at the drop surface. Such Janus drops or particles made of these drops can then be collected at the interface.[9,10] This allows emulsion stabilization and can be used in other applications.

Despite the considerable progress in the synthesis and manipulation of Janus drops, their dynamics is hardly studied, especially theoretically. Janus drop generation in a Y-junction (or a pair of junctions) is a challenging problem from a computational point of view, because of moving curved

interfaces and contact lines, intermolecular interactions of liquids with hydrophilic or hydrophobic solid walls, etc. However, even the simplest problems, such as the dynamics of a single Janus drop in a uniform or shear flow, have not been addressed yet, although such data are important to control the behavior of a Janus drop or their ensemble. Moreover, to the best of our knowledge, the corresponding experiments have also been absent so far.

The velocity of a microfluidic flow is rather small and therefore the problem can be solved within the Stokes approximation. A considerable progress is achieved in this field and the main techniques are described in classical books.[11,12] The general formalism in application to the solid particles implies finding the resistance/mobility tensors (see Ref. 13 and references therein). In other words, one has to express the force, torque, and stress tensor applied to a particle via the velocity, angular velocity, and shear rate of the flow in the absence of the particle or vice versa. Such a relation for a stick-slip particle, consisting of two patches, slip and no-slip ones, was calculated by Swan and Khair.[14] Using the boundary integral formulation, the authors derived a Faxén-type formula. In particular, they showed the coupling between a force and rotation and demonstrated that the particle can migrate parallel to the velocity gradient in a one-dimensional shear flow. A similar, though less general, problem – a particle with nonuniform slip at the surface in a uniform flow – was considered independently by Willmott.[15]

Even for a single-fluid drop such a formalism fails.[16] For instance, there is no means to couple the torque exerted on a drop with the difference between the angular velocities of the drop and the ambient. Indeed, a rotational motion of a drop, which is described by a velocity field, can hardly be associated with a single angular velocity. Moreover, the torque is created by a nonuniform force, which, in turn, generates a flow inside the drop; therefore, in contrast to a solid particle, the external influence on a drop cannot be characterized by a single vector quantity (the torque), the whole distribution of the force over the drop is needed. On the other hand, a drop in an external flow has an additional degree of freedom; the interface can deform and the position of the interface should be found along with the flow velocity. Such a coupling, generally speaking, makes the problem nonlinear even within the Stokes approximation. The only exception is the case of a weakly deformable drop (the large surface tension suppresses the interface distortion), where the flow velocity can be found for an unperturbed spherical interface and then the interface distortion is calculated.

The dynamics of a single-fluid drop in a uniform[17,18] or shear/extensional[16,19,20] flow is a classic problem. Recent progress in microfluidics has aroused a great interest in compound drops and their ensembles. Several simple types of compound drops were analyzed in a uniform external flow: (i) a thin-layer patch of one liquid on a nearly spherical drop of a different liquid,[21,22] (ii) a gas-liquid drop with gas phase partially engulfed by a motionless liquid film,[23] and (iii) concentric[24] or (iv) eccentric[25] spheres (see also the survey on compound drops in Ref. 26). The behavior of a concentric double emulsion drop in an extensional flow was investigated in Ref. 27; combining a perturbation technique and a boundary element method, the authors studied both small and finite distortions of the interfaces. This analysis allows calculating the bulk viscosity of dilute A-type multiple emulsion (a single internal drop for each external one).[27] However, the analysis of compound drops in external flows lacks in the study of such an important object as Janus drops. The present paper aims to generalize Refs. 17 and 18 to a Janus drop, a compound drop which comprises two hemispherical liquid domains.

This paper is organized as follows. We state the problem in Sec. II which consists of two subsections. In Sec. II A the existence of a compound drop close to Janus one is discussed in terms of a weak distortion from the combination of two perfect hemispheres. In Sec. II B the problem of the Stokes flow past a Janus drop is formulated. The axisymmetric problem is analyzed in Sec. III; the case, when the external flow is parallel to the internal interface, is studied in Sec. IV. We demonstrate that the velocity field (and hence the force and torque imposed on a drop) for arbitrary orientation between the internal interface and the flow can be represented as a superposition of the velocities for these two particular problems. Then, in Sec. V, we study two different situations: fixed orientation of the drop with respect to the flow (Sec. V A) and the dynamics of a torque-free drop (Sec. V B). Small deflections of the interfaces are found for the latter case in Sec. V C. Concluding remarks are presented in Sec. VI.

II. PROBLEM FORMULATION

A. Shape of equilibrium drop

Prior to analyzing the flow past a Janus drop, let us briefly discuss the conditions under which a compound drop is close to a perfect Janus drop—a combination of two hemispheres. In other words, we are interested in the situation, where (i) the internal interface is almost flat and (ii) the sum of contact angles $\alpha_1 + \alpha_2$ is close to π, see Fig. 1(a). This analysis is in a close connection with the recent paper, Ref. 28 (see also Ref. 26), but we present some additional important information for the particular case of a "half-and-half" drop. It is intuitively clear that the surface tensions have to be related as follows: $\tilde{\gamma}_{01} \approx \tilde{\gamma}_{02} \gg \tilde{\gamma}_{12}$, where $\tilde{\gamma}_{ij}$ is the surface tension at the interface between ith and jth fluids; $i = 0$ corresponds to the ambient. (Henceforth, tildes are prescribed to the dimensional characteristics.) It should be emphasized that typically the first inequality, $\tilde{\gamma}_{01} \approx \tilde{\gamma}_{02}$, ensures the second one, $\tilde{\gamma}_{01} \gg \tilde{\gamma}_{12}$.

In dimensionless form, the problem is governed by the two ratios of the surface tension:

$$\gamma_{01} = \frac{\tilde{\gamma}_{01}}{\tilde{\gamma}_{12}}, \gamma_{02} = \frac{\tilde{\gamma}_{02}}{\tilde{\gamma}_{12}}. \tag{1}$$

From the computational point of view, it is more convenient to deal with the mean interfacial tension at the external surface of the drop $\gamma = (\gamma_{01} + \gamma_{02})/2$ and the difference of the interfacial tensions, $[\gamma] = \gamma_{02} - \gamma_{01}$. Within this subsection we assume $\gamma_{02} \geq \gamma_{01}$ or $[\gamma] \geq 0$, which for the static problem can be achieved by numbering the liquids.

The base state of the compound drop in a motionless liquid is the following: the pressure in each fluid is uniform, whereas the interfaces are spherical segments.[26] For the general case, the shape of the half-and-half compound drop is determined by the following relations:

$$\frac{\gamma_{01}}{a_1} = \frac{\gamma_{02}}{a_2} - \frac{1}{a_0}, \tag{2a}$$

$$\gamma_{01} \cos\vartheta_1 = \gamma_{02} \cos\vartheta_2 - \cos\vartheta_0, \tag{2b}$$

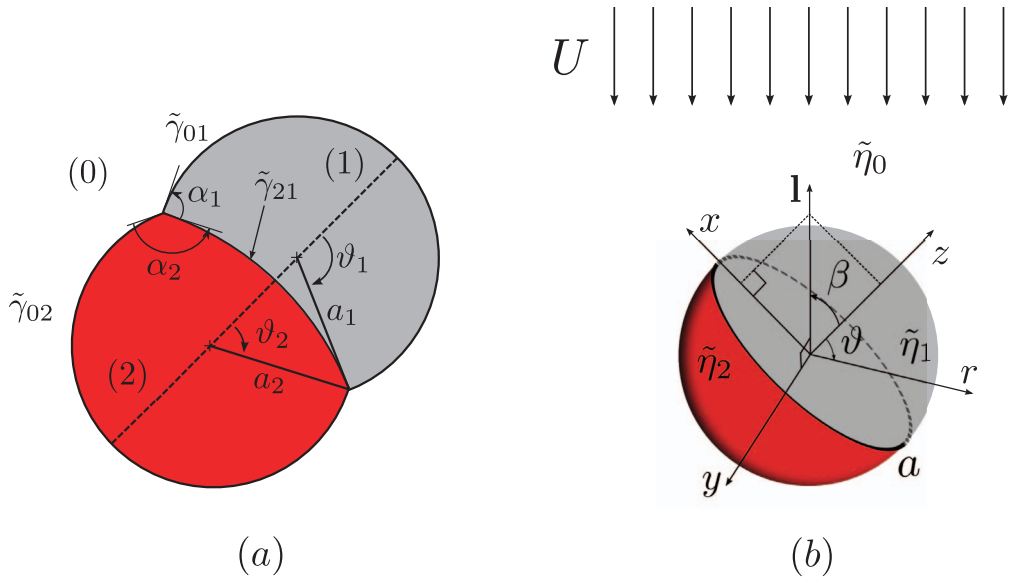

FIG. 1. Model sketches: (a) Equilibrium Janus-like drop with contact angles $\alpha_{1,2}$; the dashed line is the symmetry axis. The radius a_0 and angle ϑ_0 for the internal interface are introduced in the similar manner as $a_{1,2}$ and $\vartheta_{1,2}$, respectively. (b) A Janus drop in an external flow $-U\mathbf{l}$. The angle β indicates the drop orientation with respect to the flow: $\beta = 0$ corresponds to the internal interface normal to the external flow (axisymmetric problem, Sec. III), whereas $\beta = \pi/2$ corresponds to the internal interface parallel to the external flow (Sec. IV).

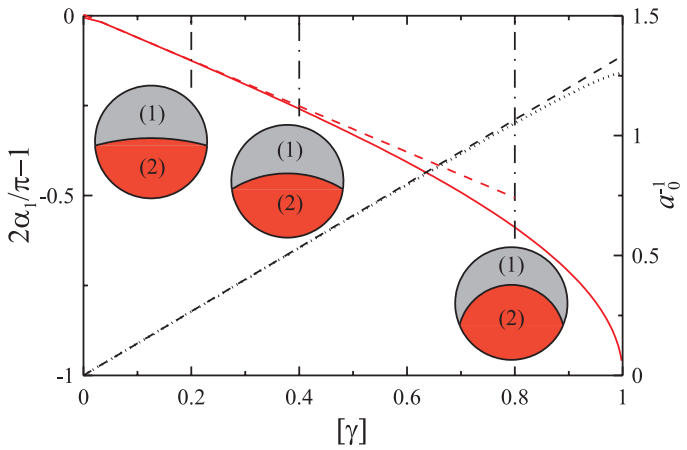

FIG. 2. Variation of the contact angle α_1 (the solid line, left axis) and the curvature of the internal interface a_0^{-1} (the dotted line, right axis) with the difference of the surface tensions $[\gamma]$ for $\gamma = 100$. The dashed lines correspond to the asymptotic formulas, Eq. (3). Vertical dashed-dotted lines indicate the values of $[\gamma]$ for which the drop shapes are shown.

$$\gamma_{01} \sin \vartheta_1 = \gamma_{02} \sin \vartheta_2 - \sin \vartheta_0, \tag{2c}$$

$$a_0 \sin \theta_0 = a_1 \sin \theta_1 = a_2 \sin \theta_2, \tag{2d}$$

$$\begin{aligned} V_{1,2} \mp V_0 &= 2, \\ V_{1,2} &= a_{1,2}^3 \left(2 \mp 2\cos \vartheta_{1,2} \mp \cos \vartheta_{1,2} \sin^2 \vartheta_{1,2}\right), \\ V_0 &= a_0^3 \left(2 - 2\cos \vartheta_0 - \cos \vartheta_0 \sin^2 \vartheta_0\right), \end{aligned} \tag{2e}$$

representing the balance of pressures, two projections of the tangential forces imposed on the triple line, obvious geometric constraint, and fixed volumes ($2\pi/3$ by the appropriate choice of the lengthscale) of each liquid, respectively. Here, ϑ_0 (a_0) is the analog of $\vartheta_{1,2}$ ($a_{1,2}$) for the internal interface which is not shown in Fig. 1(a). In fact, one out of these conditions is not independent; e.g., Eq. (2c) can be derived combining Eqs. (2a) and (2d).

For a drop close to Janus one, the above-mentioned mean surface tension is large, whereas the difference of surface tensions is small. Expanding the variables which appear in Eq. (2) with respect to both small γ^{-1} and $[\gamma]$, one can readily derive

$$\alpha_{1,2} = \frac{\pi}{2} + \frac{1}{2\gamma} \mp [\gamma], a_0^{-1} = \frac{4}{3}[\gamma]. \tag{3}$$

These approximate formulas are compared with the numerical results in Fig. 2 for different $[\gamma]$ and $\gamma = 100$. The shapes of the drops are also shown in this figure. It is clear that for $[\gamma] < 0.2$, Eq. (3) works well, and the drop can be treated as a perfect Janus one with high accuracy.

In fact so large value of γ is not needed, even for $\gamma = 5$, the calculations performed are in a good agreement with the analytical solution, Eq. (3), and only slightly differ from those shown in Fig. 2. It is worth noting that the solid line in Fig. 2 agrees well with the following formula:

$$\cos \alpha_1 = [\gamma], \alpha_2 \approx \pi - \alpha_1,$$

valid at large γ and finite $[\gamma] < 1$. (This relation can be derived by equating the tangential forces exerted on the drop interface at the triple line.) In order to calculate a_0 within the same approximation, a transcendent equation should be solved numerically; this solution agrees well with the dotted line in Fig. 2.

Thus, a real compound drop is close to the Janus one in a wide parameter range.

B. Stokes flow

Let us now consider a steady motion of a Janus drop in an external uniform flow $-U\mathbf{l}$, see Fig. 1(b). All the relaxation processes, such as damping of the initial disturbances and decay of capillary waves, are over and the terminal state is sought. For simplicity, it is assumed that each internal fluid occupies a hemispherical domain of radius a and that flow-induced deformations of the interfaces are small. Therefore, below we deal with a perfect Janus drop; for Janus-like drop, described by Eq. (3), the corrections to the flow are proportional to small $[\gamma]$ and γ^{-1} and can be calculated by means of a perturbation technique. These cumbersome calculations lie outside the scope of the current work.

Keeping in mind numerous applications of Janus drops in microfluidics, we analyze the problem in the framework of the Stokes approximation, thus seeking for the creeping flow only. In order to guarantee these conditions, one has to set both the capillary number $Ca_{12} = \tilde{\eta}U/\tilde{\gamma}_{12}$ and the Reynolds number $Re = Ua\tilde{\rho}/\tilde{\eta}$ small.[29] Here, $\tilde{\rho}$ and $\tilde{\eta}$ are the typical (for instance, the mean values) density and dynamic viscosity of the system, respectively; the minimum value of the surface tension enters Ca_{12} in order to ensure all the interfaces being nondeformable. We do not present the formal expansion in powers of Ca_{12}, just mentioning that the small $O(Ca_{12})$ interface deformations induced by the flow are slaved. These deformations can be found from the balance of normal stresses, see Sec. V C, whereas the $O(1)$ flow is calculated for the nondeformable interfaces without taking the normal stresses into account.[29]

We introduce spherical coordinates r, ϑ, ϕ [see Fig. 1(b)], which are coupled to the Cartesian coordinates in the usual way. The x-axis is chosen in such a manner that the external flow (or vector $\mathbf{l}$) is parallel to the x–z plane and $l_x \geq 0$ (l_x vanishes for the axisymmetric problem, see Sec. III); the y-axis is directed so as to make the coordinate system a right-handed one. The boundary value problem governing the drop dynamics reads

$$\nabla \cdot \mathbf{v}^{(j)} = 0, \; -\nabla p^{(j)} + \eta_j \nabla^2 \mathbf{v}^{(j)} = 0, \tag{4a}$$

$$v_n^{(j)} = 0, \; [\mathbf{v}_\tau] = [\sigma_{n\tau}] = 0 \text{ at } r = 1, \tag{4b}$$

$$v_n^{(1,2)} = 0, \; [\mathbf{v}_\tau] = [\sigma_{n\tau}] = 0 \text{ at } \vartheta = \frac{\pi}{2}, \tag{4c}$$

$$\mathbf{v}^{(0)} = -\mathbf{l} \text{ at } r \gg 1. \tag{4d}$$

Here, j is each of the numbers 0, 1, 2; $j = 0$ is again prescribed to the ambient, see Fig. 1(b), whereas in contrast to Sec. II A for the internal fluids the inequality $\tilde{\eta}_1 \leq \tilde{\eta}_2$ holds true. (Thus, the choice of the first and second fluids in Sec. II A can differ from that in the rest of the paper.) The vectors $\mathbf{n}$ and τ are, respectively, normal and tangential to the corresponding interface. (For the general case, τ-component of the velocity is a two-dimensional vector field.) The stress tensor is Newtonian: $\sigma_{lk}^{(j)} = \eta_j(\nabla_l v_k^{(j)} + \nabla_k v_l^{(j)}) - p^{(j)}\delta_{lk}$. The brackets denote a jump in the corresponding characteristics across the interface; the direction of this jump will be specified, wherever needed. Later on we will not use the brackets in formulas for any other purposes. All the remaining notations are conventional.

The problem is written in the dimensionless form with U, a, and $\tilde{\eta}_0 U/a$ used as the scales for the velocity, length, and pressure, respectively. Therefore, $\eta_0 = 1$ in Eq. (4), whereas $\eta_{1,2} = \tilde{\eta}_{1,2}/\tilde{\eta}_0$ are the dimensionless parameters of the problem. The third dimensionless parameter defines the unit vector $\mathbf{l} = (\sin\beta, 0, \cos\beta)$, $0 \leq \beta \leq \pi$, which indicates the mutual orientation of the drop and the external flow. Two limiting orientations, $\beta = 0$ (or $\beta = \pi$) and $\beta = \pi/2$, are analyzed in Secs. III and IV, respectively. Due to linearity of the problem, the solution for any intermediate case can be represented as a combination of these two cases.

The objective is to calculate the flows past and inside the drop, the force $\mathbf{F}$ imposed on the drop (in units $\tilde{\eta}_0 aU$)

$$\mathbf{F} = \oint \sigma \cdot \mathbf{n} \mathrm{d}S, \tag{5}$$

and the torque $\mathbf{T}$ (nondimensionalized by means of $\tilde{\eta}_0 a^2 U$)

$$\mathbf{T} = \oint \mathbf{r} \times (\sigma \cdot \mathbf{n}) \mathrm{d}S, \tag{6}$$

where the integrations are performed over the drop surface, $r = 1$.

Two practically important situations are possible: (i) the fixed drop, which can neither move nor rotate under external force and torque and (ii) the torque-free drop, which is oriented so that the total torque vanishes. In other words, β is kept fixed for case (i) and $\beta = \beta_{eq}$ has to be calculated for case (ii). It is intuitively clear that for case (ii) β_{eq} is either zero or π and the former value, $\beta_{eq} = 0$, corresponds to the stable state. Let us imagine an occasional increase in β from zero value to the situation sketched in Fig. 1(b). It enhances the area of the more viscous fluid on the left-hand side of the drop, whereas on the right-hand side the area of the less viscous fluid increases. Therefore, the viscous drag on the former part becomes larger and an overall torque inhibits the initial turn. In contrast, for $\beta = \pi$ the resulting torque increases the initial perturbation. A more rigorous analysis of the situation is carried out in Sec. V B.

III. AXISYMMETRIC FLOW

A. Vector potential formulation

For $\beta = 0$ the problem becomes two-dimensional and therefore the vector potential ψ can be introduced:

$$\mathbf{v} = \nabla \times \left\{ \psi(r, \vartheta) \mathbf{e}_\phi \right\} \tag{7}$$

or, in components,

$$v_r = \frac{1}{r \sin \vartheta} \partial_\vartheta \left(\sin \vartheta \, \psi \right), \; v_\vartheta = -\frac{1}{r} \partial_r (r \psi).$$

It is worth noting that ψ is coupled with the conventional Stokes streamfunction[11] ψ_c (associated with the flow streamlines) according to the relation

$$\psi_c = r \sin \vartheta \, \psi. \tag{8}$$

In terms of the vector potential, the boundary value problem, Eq. (4), is rewritten as follows:

$$D^2 \psi^{(j)} = 0, \tag{9a}$$

$$\psi^{(j)} = 0, \, [\partial_r \psi] = \left[\eta \partial_r^2 \psi \right] = 0 \text{ at } r = 1, \tag{9b}$$

$$\psi^{(1,2)} = 0, \, [\partial_\vartheta \psi] = \left[\eta \partial_\vartheta^2 \psi \right] = 0 \text{ at } \vartheta = \frac{\pi}{2}, \tag{9c}$$

$$\psi^{(0)} = -\frac{r}{2} \sin \vartheta \text{ at } r \gg 1. \tag{9d}$$

The operator D is introduced by the following relation:

$$Df = \nabla^2 f - \frac{1}{r^2 \sin^2 \vartheta} f$$

for any $f(r, \vartheta)$.

We represent the vector potentials of the ambient as follows:

$$\psi^{(0)} = \sum_{n=1}^{\infty} \frac{A_n P_n^{(1)}(\theta)}{r^{n+1}} \left(1 - r^2\right) + \psi_S, \; \psi_S = \frac{1}{4} \left(3 - \frac{1}{r^2} - 2r \right) \sin \vartheta, \tag{10}$$

where $\theta = \cos \vartheta$, ψ_S corresponds to the flow past a solid sphere, and $P_n^{(1)}$ is the associate Legendre polynomial:

$$P_n^{(1)}(\theta) = \sqrt{1 - \theta^2} \frac{d P_n(\theta)}{d\theta},$$

i.e., in the notations of Ref. 30, we use $P_{n1} = -P_n^1$ as the associate Legendre polynomials.

Inside the drop the vector potentials are given by

$$\psi^{(1,2)} = \eta_{2,1} \sum_{n=1}^{\infty} \{B_n T_n(\theta) \pm C_n r R_n(\theta)\} r^{2n+1} + \sum_{n=1}^{\infty} D_n P_{2n}^{(1)}(\theta) r^{2n} \left(1 - r^2\right), \tag{11}$$

$$T_n = \frac{P_{2n+1}^{(1)}(\theta)}{P_{2n+1}^{(1)}(0)} - \frac{P_{2n-1}^{(1)}(\theta)}{P_{2n-1}^{(1)}(0)}, \quad R_n = \frac{P_{2n+2}^{(1)}(\theta)}{Q_{2n+2}(0)} - \frac{P_{2n}^{(1)}(\theta)}{Q_{2n}(0)}, \tag{12}$$

where $Q_n = \theta P_n' - n(n+1)P_n$ and therefore $Q_{2n}(0) = -2n(2n+1)P_{2n}(0)$.

The vector potential given by Eq. (10) solves the biharmonic equation, Eq. (9a), ensures both vanishing $\psi^{(0)}$ at $r = 1$ and correct asymptotics far from the drop, whereas $\psi^{(1,2)}$ given by Eq. (11) satisfy Eq. (9a) and the boundary conditions at $\vartheta = \pi/2$.

Substituting this ansatz for $\psi^{(j)}$ into the remaining boundary conditions at $r = 1$ and cutting the series at $2N$th spherical harmonics, one arrives at a set of $5N$ linear algebraic equations for $5N$ coefficients: A_n $(1 \le n \le 2N)$ and B_n, C_n, D_n $(1 \le n \le N)$. This set of equations is solved numerically. In order to guarantee the convergence, N is chosen from 60 to 120 depending on η_1 and η_2; more terms should be retained for the case $\eta_2 \gg 1 \gg \eta_1$ (or $\tilde{\eta}_2 \gg \tilde{\eta}_0 \gg \tilde{\eta}_1$). An example of such a system is provided by a toy Janus "drop" which comprises a solid and a gaseous hemisphere. It is worth noting that in most microfluidic applications the viscosities of all three fluids are relatively close. Therefore, the limiting case $\eta_2 \gg 1 \gg \eta_1$ seems to be unimportant from practical point of view. Involving the higher order Legendre polynomials inevitably leads to additional care about round-off errors, hence the number of digits in computations has to be increased. Finally, it should be noted that the series for the stress tensor converges nonuniformly, but no singularities take place for the motionless triple line.

For the axisymmetric case the force given by Eq. (5) has the only component $F_z = 2\pi(3 - 4A_1)$, which agrees with the classical expression by Payne and Pell.[31] (F_z is directed against the z-axis; here and below we omit the sign of the force.) The overall torque, Eq. (6), vanishes in view of the obvious symmetry arguments.

B. The limiting case $\eta_1 = \eta_2$

First we stress that even in the limiting case of equal internal viscosities $\eta_1 = \eta_2 = \eta$ {here and below $\eta = (\eta_1 + \eta_2)/2$ is the mean viscosity of the drop}, the problem does not reduce to a uniform flow past a drop studied by Hadamard[17] and Rybczynski.[18] Indeed, the nondeformable interface inside the drop prohibits the motion found in the cited papers. Thus, right away, one can expect that a Janus drop is intermediate between a single-fluid drop and a solid particle in terms of hydrodynamic resistance. Mathematically, the problem is simplified in the limiting case $\eta_1 = \eta_2$, because the coefficients D_n and A_{2n} vanish to ensure that the solution is even in θ or, in other words, to guarantee the symmetry properties $\psi(r, \vartheta) = \psi(r, \pi - \vartheta)$. Particularly, this shows that both velocity components vanish at the internal interface. Calculations of the force acting on the drop are shown in Fig. 3(a), and these are compared against the Hadamard–Rybczynski formula

$$F_z = 2\pi \frac{2 + 3\eta}{1 + \eta}. \tag{13}$$

As can be seen from the figure, for any given η, the force imposed on the drop lies in between the force on a rigid particle $F_z = 6\pi$, and the force given by the Hadamard–Rybczynski formula, Eq. (13). It is also clear that the force F_z grows from 4π (low viscosity drop) to 6π (high viscosity drop), as η ranges from zero to infinity. (In these two limiting cases, the internal interface produces negligible effect.) It should be mentioned that similar results, the force varying between the Hadamard–Rybczynski formula to the Stokes one, were also found in a number of systems, such as compound drops[22,24] and drop motion in the presence of surfactants.[32]

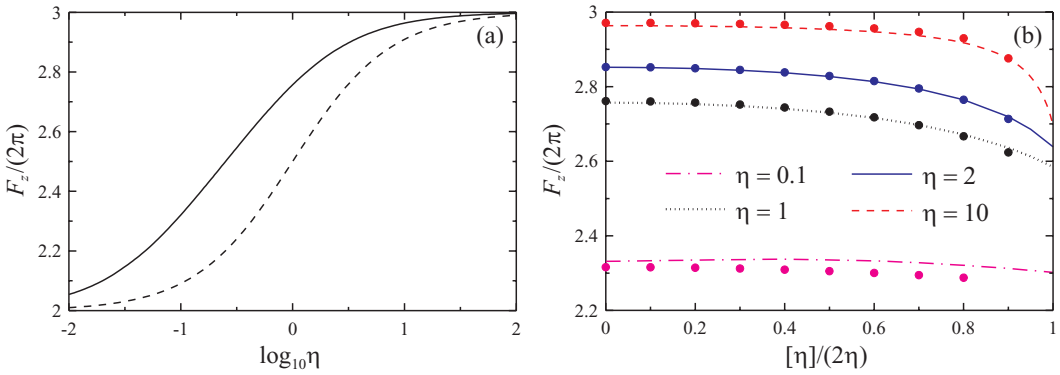

FIG. 3. The force $F_z/(2\pi)$ (in units $\tilde{\eta}_0 aU$) imposed on the Janus drop. (a) Variation of $F_z/(2\pi)$ with η for $\eta_1 = \eta_2 = \eta$. The solid line represents numerical results; the dashed line shows the Hadamard–Rybczynski formula, Eq. (13). (b) Variation of $F_z/(2\pi)$ with $[\eta]/(2\eta) = (\eta_2 - \eta_1)/(\eta_1 + \eta_2)$ for various mean viscosities of the drop $\eta = (\eta_1 + \eta_2)/2$; results of DNS (ANSYS Fluent) are shown by the dots.

C. Different internal viscosities

For different viscosities η_1 and η_2 it is useful to present the results in terms of the mean drop viscosity η and the viscosity difference, $[\eta] = \eta_2 - \eta_1$. Keeping in mind that $[\eta] \le 2\eta$ for any η, one can conclude that the weighted viscosity difference $[\eta]/(2\eta)$ is more convenient for presentation purposes. It is easy to show that $\eta_{1,2} = \eta\{1 \mp [\eta]/(2\eta)\}$. The results of calculations for nonzero $[\eta]$ are presented in Fig. 3(b). As one can see from this figure, the force slightly depends on the redistribution of this "average" viscosity between the internal fluids. Indeed, at $[\eta] \le \eta$ the variation of the force does not exceed 1%. Recalling that in most microfluidic applications the viscosity contrast inside the drop is rather small, one can conclude that Fig. 3(a) provides a good approximation of the force imposed on the drop.

With further increase in $[\eta]$ the force becomes smaller. Note that the case $\eta_2 \gg \eta_1$ ($2\eta \approx [\eta]$) should be thought of as a combination of two liquids with a large difference in the viscosities rather than a liquid-gas pair. In the latter case, there is no means to sustain a Janus drop. The force diminution is especially pronounced for the extremal situation $\eta_2 \gg 1 \gg \eta_1$, which, as we stated above, is not practically important.

The flow inside and outside the drop is demonstrated in Fig. 4; keeping in mind the axial symmetry, one concludes that a couple of toroidal vortices appear inside the drop. It should be noticed that the ϑ-component (longitudinal) of the velocity at the drop surface is non-negative; thus, both liquids are co-rotating; the vorticities (or the vector potentials) are of the same sign in both hemispheres. Such a system of vortices ensures a correct velocity matching at the drop surface, but it leads to counter-propagating flows at the internal interface, which is obviously impossible. In order to prevent such an effect, an additional vortex appears in a less viscous liquid near the internal interface. Its boundary is plotted by the unclosed streamline adjacent to the internal interface. The intensity of this counterflow is rather small and the streamlines cannot be shown on the scale of Fig. 4. It is evident that for the limiting case $[\eta] = 0$ the additional vortex is not needed because the longitudinal components of the velocity are zero at the internal interface.

It is readily seen that the intensity of the flow in the drop is much smaller than in the surrounding fluid; the step between the isolines is ten times smaller in the former case. This effect is mainly caused by the above-mentioned additional hindrance to the flow in the drop owing to the internal interface. Another evident result is that the flow is more intensive in the first (less viscous) liquid.

As we have noted above, the convergence of the series, Eqs. (10) and (11), for the vector potentials is rather slow. In order to confirm the results independently, we also perform direct numerical simulations (DNS) by means of ANSYS Fluent software. To that end we solve the problem inside a spherical domain $r = 20$ with a space-uniform velocity kept fixed at the external boundary of the domain. Nonuniform tetrahedral mesh comprising 52 000 cells is used with a refinement

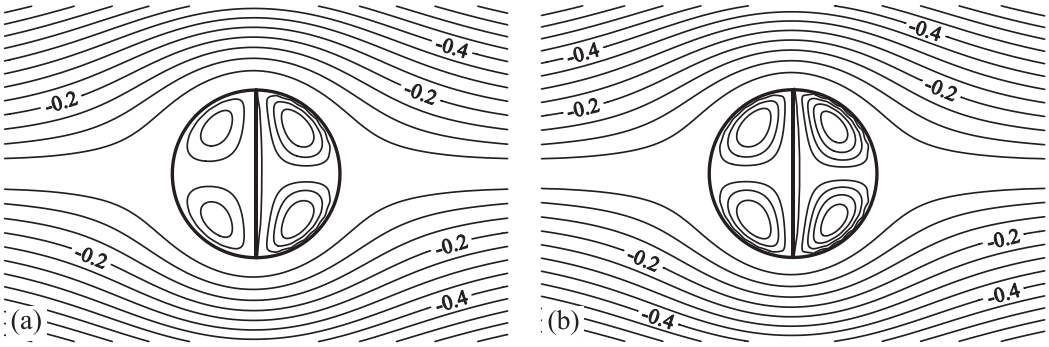

FIG. 4. The isolines of the velocity potential ψ for axisymmetric flow, $\eta_2 = 1.5, \eta_1 = 0.5$ (a) and $\eta_2 = 0.7, \eta_1 = 0.3$ (b). The step between the isolines is 0.05 for the external flow and 0.005 inside the drop.

near the drop interface. We use Body Force Weighted scheme for pressure spatial discretization and Third-Order MUSCL scheme for the momentum equation. ANSYS Fluent offers the Volume-of-fluid (VOF) method for modeling two or more immiscible fluids by solving a single set of momentum equations and tracking the volume fraction of each fluid over the domain. However, this model is inconvenient for nondeformable interfaces. Therefore, we use the simplified approach when, similarly to the conventional level set method, the transient layer is introduced near the interfaces, but the equation for level set function is not solved, which keeps the interfaces fixed. In order to satisfy the boundary conditions, additional source terms are added, which prevent the fluid motion across the interfaces. The Reynolds number $Re_0 = Ua/\tilde{\eta}_0$ in computations is chosen 0.1. The results of DNS are presented in Fig. 3(b) and they are in a good agreement with the analytical approach. The difference of the results becomes more pronounced in the above-mentioned case $\eta_2 \gg 1 \gg \eta_1$ ($[\eta] \approx 2\eta \gg 1$), which is the most complicated from computational point of view but practically unimportant.

It is also clear that no separate analysis is needed for $\beta = \pi$; this limiting case corresponds to the opposite direction of the external flow, which, in view of linearity, only changes the sign of the force keeping its absolute value fixed.

IV. EXTERNAL FLOW, PARALLEL TO THE INTERNAL INTERFACE ($\beta = \pi/2$)

In the case $\beta = \pi/2$ the second (more viscous) fluid is assumed to be situated at $z < 0$, i.e., the flow directed oppositely to the x-axis has to produce the torque parallel to the y-axis. (The replacement of fluids 1 and 2 only changes the sign of the torque.) For this particular case, the calculations are more complicated because of the three-dimensional structure of the velocity fields. To that end, we implement the Lamb representation of the velocity, see also Refs. 11 and 12:

$$\mathbf{v}^{(j)} = \nabla \times \left(\mathbf{r}\chi^{(j)}\right) + \nabla\Phi^{(j)} + \nabla^{-2}\left(\nabla\bar{p}^{(j)}\right) + \mathbf{v}_\infty^{(j)}, \tag{14}$$

where ∇^{-2} is the inverse of the Laplace operator, $\bar{p}^{(j)} = p^{(j)}/\eta_j$, $\mathbf{v}_\infty^{(0)} = -\mathbf{l}$ far from the drop. From the computational point of view, it is convenient to choose $\mathbf{v}_\infty^{(1,2)} = 0$ at the drop surface, i.e., $\mathbf{v}_\infty^{(0)}$ is the Stokes flow past a solid sphere of unit radius. The components of this field are given by

$$v_{\infty r}^{(0)} = -L(r)\sin\vartheta\cos\phi,\ v_{\infty\vartheta}^{(0)} - M(r)\theta\cos\phi,\ v_{\infty\phi}^{(0)} = M(r)\sin\phi, \tag{15}$$

$$L(r) = 1 - \frac{3}{2r} + \frac{1}{2r^3},\ M(r) = 1 - \frac{3}{4r} - \frac{1}{4r^3}. \tag{16}$$

Scalar Lamb's functions χ, Φ, and $\bar{p}$ solve Laplace's equation. The series for these functions as well as for the velocity fields are given in Appendix A.

A. Small viscosity difference

For arbitrary $[\eta]$, calculations are massive but in the limiting case of small $[\eta]/\eta$ (recall, $[\eta] = \eta_2 - \eta_1$) a certain simplification is possible. Indeed, for equal internal viscosities the problem is reduced to that solved by Hadamard[17] and Rybczynski.[18] The corresponding solution reads

$$v_r^{(1,2)} = V_r^{(1,2)} \equiv \mu(1 - r^2)\sin\vartheta\cos\phi, \tag{17a}$$

$$v_\vartheta^{(1,2)} = V_\vartheta^{(1,2)} \equiv \mu(1 - 2r^2)\cos\vartheta\cos\phi, \tag{17b}$$

$$v_\phi^{(1,2)} = V_\phi^{(1,2)} \equiv -\mu(1 - 2r^2)\sin\phi, \tag{17c}$$

$$v_r^{(0)} = V_r^{(0)} \equiv -\left(1 + \frac{\alpha}{r} + \frac{\nu}{r^3}\right)\sin\vartheta\cos\phi, \tag{17d}$$

$$v_\vartheta^{(0)} = V_\vartheta^{(0)} \equiv -\left(1 + \frac{\alpha}{2r} - \frac{\nu}{2r^3}\right)\cos\vartheta\cos\phi, \tag{17e}$$

$$\begin{gathered} v_\phi^{(0)} = V_\phi^{(0)} \equiv \left(1 + \frac{\alpha}{2r} - \frac{\nu}{2r^3}\right)\sin\phi, \\ \mu = \frac{1}{2(1+\eta)}, \alpha = -\frac{2+3\eta}{2(1+\eta)}, \nu = \frac{\eta}{2(1+\eta)}. \end{gathered} \tag{17f}$$

In this case the x-component of the force is given by the classic expression, Eq. (13), and there is no torque applied to the drop.

At small $[\eta]/\eta$ the velocity fields $\mathbf{V}^{(j)}$, Eq. (17), should be supplemented by the $O([\eta]/\eta)$-correction $\mathbf{u}^{(j)}$. Such a correction obviously solves the boundary value problem similar to Eqs. (4) with the replacement of the shear stress balance at $r = 1$ by

$$\partial_r \frac{\eta u_\vartheta^{(1,2)} - u_\vartheta^{(0)}}{r} = \pm\eta\partial_r \frac{V_\vartheta}{r}, \quad \partial_r \frac{\eta u_\phi^{(1,2)} - u_\phi^{(0)}}{r} = \pm\eta\partial_r \frac{V_\phi}{r}, \tag{18}$$

where the upper (lower) sign is prescribed to the interface between the ambient and the first (second) fluid. The first correction obeys an additional symmetry condition

$$\left\{u_r^{(0,1)}, u_\vartheta^{(0,1)}, u_\phi^{(0,1)}\right\}_\vartheta = \left\{-u_r^{(0,2)}, u_\vartheta^{(0,2)}, -u_\phi^{(0,2)}\right\}_{\pi-\vartheta}, \tag{19}$$

so that the meridional components of the velocity coincide in both internal fluids, whereas the radial and azimuthal components are opposite. This symmetry property simplifies the analysis to a great extent, although numerical summation is still needed; the details of calculations are presented in Appendix B. It ensues from the analysis presented there that the force does not have $O([\eta]/\eta)$ correction but the torque does. This correction is presented in Fig. 5.

It can be readily seen from the figure that the torque is maximum for a certain value of η and it tends to zero in two opposite limits of small and large η. Again, the former case should be thought of as a water-like drop in an oil rather than a bubble in a liquid, because two gases cannot form an internal interface. The reason for vanishing T_y in this case is clear, the viscous stress is almost zero at the drop surface. The pressure field, which produces a force directed to the drop center, clearly does not create a torque. Mathematically, this vanishing stems from the factor η on the right-hand side of Eq. (18). In the latter case, for large η, the right-hand side of Eq. (18) remains finite despite the large factor η because the velocities of the internal fluids are small, see Eq. (17). Moreover, $\mathbf{u}^{(j)}$ is inversely proportional to η, even for the ambient, in order to ensure the balance of shear stresses. Therefore, e.g., $\partial_r(u_\vartheta^{(1)}/r)$ is equal to $\partial_r(V_\vartheta^{(1)}/r)$ at $r = 1$, whereas the $O([\eta]/\eta)$ correction to the stress produced by the surrounding fluid can be disregarded. (The correction to the velocity in the ambient can then be found from the velocity continuity at $r = 1$.) In both limiting cases of small and large η, the asymptotics η and η^{-1} agree well with the numerical values presented in Fig. 5.

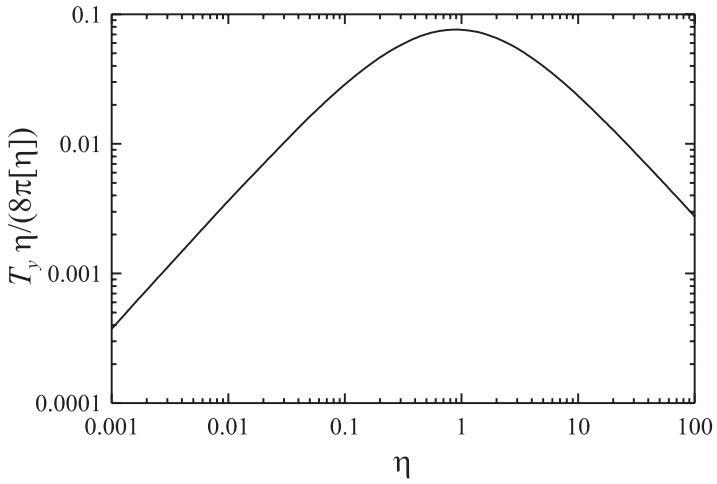

FIG. 5. Variation of the rescaled torque $T_y\eta/(8\pi[\eta])$ (in units $\tilde{\eta}_0 a^2 U$) acting on the Janus drop for small $[\eta]/(2\eta) = (\eta_2 - \eta_1)/(\eta_1 + \eta_2)$ with the mean viscosity of internal fluids $\eta = (\eta_1 + \eta_2)/2$.

B. Finite viscosity difference

For arbitrary value of $[\eta]/\eta$, the full three-dimensional representation of the velocities given in Appendix A is used. The results of calculations are presented in Fig. 6. At small $[\eta]/\eta$ the torque agrees well with the results shown in Fig. 5. For $\eta = 0.1$, the coincidence is good even for $[\eta]/(2\eta)$ close to unity. With increase in the mean viscosity of the drop, the domain of applicability of the results for small $[\eta]/(2\eta)$ shrinks; the nonlinear corrections augment the total torque. As one can expect, the convergence of the series becomes worse with increase in the viscosity contrast; again this effect is especially pronounced for larger η.

In Fig. 6(b) the force exerted on the Janus drop is depicted. According to the analysis at small $[\eta]$, the correction to Eq. (13) is quadratic in terms of $[\eta]$. Moreover, at small and moderate mean viscosity of the drop the force is almost independent of the viscosity contrast; for example, at $\eta = 1$, the force variation remains within 10%, whereas the weighted viscosity difference $[\eta]/(2\eta)$ increases from zero to its maximal value, unity.

We also perform the DNS in 3D case, the results are presented in Fig. 6(b); the forces obtained within two approaches agree well; similarly to the axisymmetric case the discrepancy grows as $[\eta]/(2\eta)$ tends to unity, cf. Fig. 3(b).

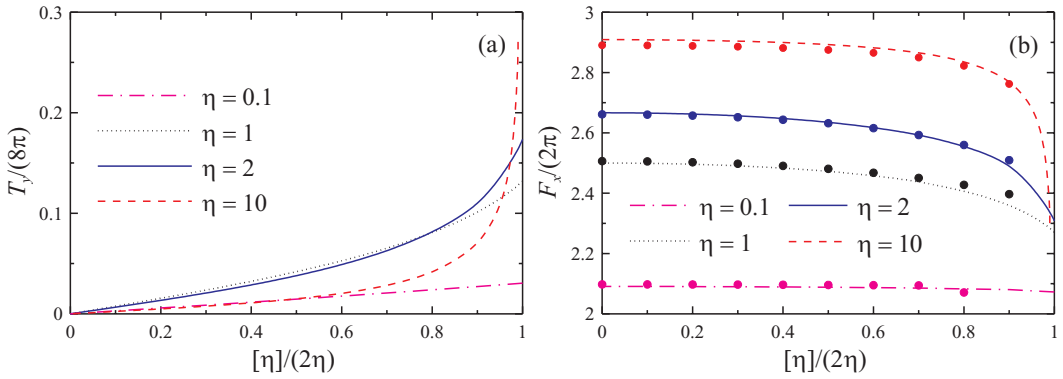

FIG. 6. Variation of the torque $T_y/(8\pi)$ (in units $\tilde{\eta}_0 a^2 U$) (a) and the force $F_x/(2\pi)$ (in units $\tilde{\eta}_0 a U$) (b) imposed on the Janus drop with $[\eta]/(2\eta) = (\eta_2 - \eta_1)/(\eta_1 + \eta_2)$ for different mean viscosities η of the drop. Results of DNS (ANSYS Fluent) are shown by the dots.

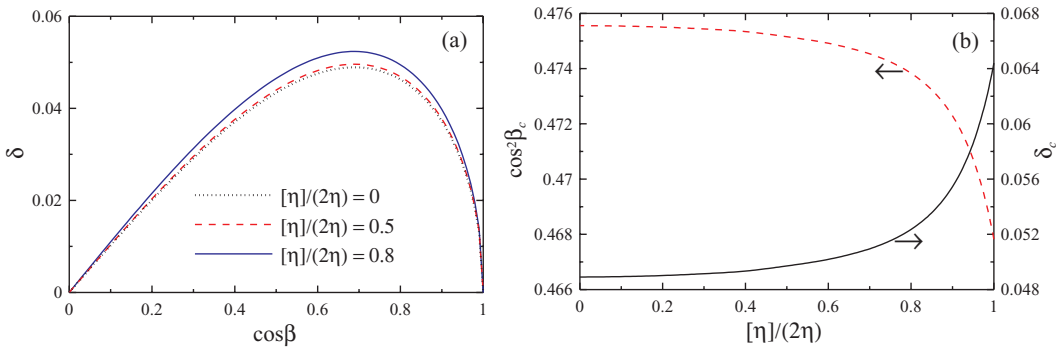

FIG. 7. Force acting on a fixed Janus drop for $\eta = (\eta_1 + \eta_2)/2 = 1$. (a) Variation of the angle δ between the external flow and force on the drop with $\cos\beta$ for different $[\eta]/(2\eta)$, see Eq. (20). (b) Variation of the maximum angle δ_c in radian (the solid line, right axis) and the value of β_c for which δ reaches its maximum (the dashed line, left axis) with the weighted viscosity difference $[\eta]/(2\eta)$, see Eq. (21).

V. DYNAMICS OF THE JANUS DROP

A. The force for the arbitrary β (fixed drop)

Below, on the ground of Secs. III and IV we address the dynamics of a Janus drop, starting with the simplest case, where both the position and orientation of the drop (the angle β) are fixed by certain external force and torque. Analysis of the more realistic situation, motion of a freely rotating drop under a prescribed external force, is postponed to Sec. V B.

It is clearly seen from Figs. 3(b) and 6(b) that the analogs of the Hadamard–Rybczynski force for two orientations of the Janus drop depend on the viscosities η_1 and η_2 in a qualitatively similar manner. However, they do not coincide exactly, which means that the force applied to a fixed drop is *not parallel* to the flow. (It should be emphasized that for a half-and-half stick-slip sphere,[14,15] the force is always parallel to the velocity.) The simple calculation shows that the angle δ between the vector $-\mathbf{l}$ and the total force $\mathbf{F}$ is given by

$$\cos\delta = \frac{F_x + (F_z - F_x)\cos^2\beta}{\sqrt{F_x^2 + (F_z^2 - F_x^2)\cos^2\beta}}. \tag{20}$$

With increase in β from zero to $\pi/2$, this angle reaches its maximum value δ_c at $\beta = \beta_c$, where

$$\cos\delta_c = \frac{2\sqrt{F_x F_z}}{F_x + F_z}, \quad \cos^2\beta_c = \frac{F_x}{F_x + F_z}. \tag{21}$$

An example of calculations is presented in Fig. 7. One can readily see that the angle between the force and the velocity does not exceed 0.065 rad or 3.7°. Another important feature is that the angle is mainly determined by the mean viscosity η; the variation of δ with the weighted viscosity difference is almost absent at $[\eta]/(2\eta) < 0.75$.

B. Stable regime for a freely rotating drop

Now we proceed with the more realistic situation of the drop moving by the action of an external force without imposing a torque. In this situation the drop should be torque-free, i.e., it is oriented in such a way that the internal interface is perpendicular to the external flow. One has only to choose between two opposite possibilities, $\beta_{eq} = 0$ and $\beta_{eq} = \pi$. As stated above, simple physical intuition dictates that the former state is stable. In fact, calculations performed in Sec. IV allow presenting more rigorous arguments. Indeed, let us imagine that the drop with the equilibrium angle $\beta_{eq} = 0$ occasionally gets a small gain in β. Therefore, in addition to the axisymmetric flow there appears a small 3D component with the velocity proportional to $U\sin\beta$. Since, similarly to the situation shown in Fig. 6(b), $z > 0$ corresponds to the first (less viscous) fluid, the y-component of the torque is positive. Thus, the viscous torque rotates the drop back trying to decrease the initial distortion. In

the opposite case, $\beta_{eq} = \pi$, the first (less viscous) fluid is situated at $z < 0$, i.e., the y-component of the torque is negative and it increases the initial perturbation of the angle.

A more subtle situation takes place for the sedimentation of the Janus drop under the action of gravity; an example of Janus drop motion under gravity can be found in Ref. 33. Dealing with the sedimentation, we assume the dimensionless mean drop density $\rho = (\tilde{\rho}_1 + \tilde{\rho}_2)/(2\tilde{\rho}_0)$ larger than unity. If, oppositely to the viscosity difference ($\eta_1 < \eta_2$) the first fluid is more dense, the terminate state remains the same, with the less viscous fluid at the upstream half. At the opposite ratio of the densities, $\tilde{\rho}_1 < \tilde{\rho}_2$, there appears a competition between the viscous and gravitational torques. Since both torques are proportional to $\sin\beta$, nontrivial equilibrium states are impossible and either $\beta_{eq} = 0$ or $\beta_{eq} = \pi$ in the stable state. The former situation occurs, when the viscosity "wins," i.e., $\tilde{\eta}_0 \tilde{U} a^2 T_y > (3/8)[\rho]\tilde{\rho}_0 g a V/2$, where $\tilde{U} = mg/(\tilde{\eta}_0 a F_z)$ is the velocity of the drop sedimentation, V and $m = (\tilde{\rho}_1 + \tilde{\rho}_2)V/2$ are the volume and mass of the drop, respectively; $[\rho] = (\tilde{\rho}_2 - \tilde{\rho}_1)/\tilde{\rho}_0$.

Thus, $\beta_{eq} = 0$ corresponds to the stable sedimentation under the condition

$$T_y > \frac{3}{16} F_z \frac{[\rho]}{\rho}, \tag{22}$$

otherwise, the opposite regime with $\beta_{eq} = \pi$ is stable.

In the opposite case of rising drop ($\rho < 1$), only the sign on the right-hand side of Eq. (22) should be changed, because in this case the two torques compete for $\tilde{\rho}_1 > \tilde{\rho}_2$.

C. Deformation of the internal interface

In the previous analysis, we have neglected the deformations of the interfaces by assuming the surface tension (or inverse capillary numbers) asymptotically large. In this subsection, small deformations of the interfaces are calculated by means of a perturbation technique. To that end, we calculate the pressure field via the Stokes equation with already known $\mathbf{v}^{(j)}$ and take into account the normal stress balance conditions.[29]

As demonstrated in Sec. II A, two fluids (1 and 2) form a Janus drop suspended in a third fluid (0), when $\tilde{\gamma}_{01} \approx \tilde{\gamma}_{02} \gg \tilde{\gamma}_{12}$. It means that the external surface of the drop remains almost nondeformable, whereas the internal interface can be distorted more easily. Mathematically, the ratio of these deformation is proportional to small $\gamma^{-1} = 2\tilde{\gamma}_{12}/(\tilde{\gamma}_{01} + \tilde{\gamma}_{02})$; therefore, only the deformation of the internal interface is studied below. Recall that for finite γ^{-1} the drop is not perfect Janus one even without any flow, see Eq. (3). The analysis is restricted to the axisymmetric case, which is shown to be more relevant from a physical point of view, see Sec. V B.

The internal interface is determined by the equation $z = \zeta(r)$, where the function $\zeta(r)$ has to be found from the balance of normal stresses:

$$\begin{gathered}[p - \sigma_{\vartheta\vartheta}] = -Ca_{12}^{-1}\Delta\zeta, \text{ at } \vartheta = \frac{\pi}{2}; \\ \Delta = \frac{1}{r}\frac{d}{dr}\left(r\frac{d}{dr}\right),\end{gathered} \tag{23}$$

where $[f] = (f_2 - f_1)_{z=0}$. Recall that the capillary number is small, $Ca_{12} = \tilde{\eta}_0 U/\tilde{\gamma}_{12} \ll 1$. The interface deformation ζ is of order Ca_{12}, which justifies the calculation based on the unperturbed interfaces and velocity fields.

Equation (23) has to be supplemented by the conditions

$$\zeta = 0 \text{ at } r = 1, \tag{24}$$

$$\int_0^1 \zeta r \mathrm{d}r = 0. \tag{25}$$

The former condition, Eq. (24), guarantees that the triple line remains unperturbed because of the strong inequality $\tilde{\gamma}_{12} \ll \tilde{\gamma}_{01} \approx \tilde{\gamma}_{02}$. (In fact, the triple line displacement is proportional to both Ca_{12} and γ^{-1}, thus vanishing in the order of approximation used here.) The latter condition, Eq. (25), fixes the volumes of each internal fluid.

The pressure fields corresponding to the vector potentials of internal fluids given by Eq. (11) have the following forms:

$$p^{(1,2)} = -2\eta_1\eta_2 \sum_{n=1}^{\infty} 2n(4n+1)B_n \frac{P_{2n-1}(\theta)}{P_{2n-1}^{(1)}(0)} r^{2n-1}$$
$$-2\eta_{1,2} \sum_{n=1}^{\infty} (2n+1)(4n+3) \left\{ D_n \pm \frac{\eta_{2,1} C_n}{Q_{2n}(0)} \right\} P_{2n}(\theta) r^{2n} + p_0^{(1,2)}, \tag{26}$$

whereas the normal viscous stress is given by

$$\sigma_{\vartheta\vartheta}^{(1,2)} \left(\vartheta = \frac{\pi}{2} \right) = -2\eta_{1,2} \sum_{n=1}^{\infty} 2n(2n+1) D_n P_{2n}(0) r^{2n-2} \left\{ 2n - r^2(2n+2) \right\}. \tag{27}$$

It is worth noting that the series terms in the pressure field do not contain contributions independent of r, whereas $\sigma_{\vartheta\vartheta}$ does contain a constant proportional to $[\eta]$. However, the latter constant just renormalizes the difference $[p_0] = p_0^{(2)} - p_0^{(1)}$ and for brevity it is neglected below. (Recall that the absolute value of the pressure is obviously unimportant for incompressible liquids, only the pressure difference plays a role.)

Solution to Eq. (23) is given by

$$\zeta = Ca_{12} \left\{ \sum_{n=1}^{\infty} \frac{Z_n}{(2n+2)^2} + \frac{[p_0]}{4} r^2 + \zeta_0 \right\},$$
$$Z_n = -2\eta_1\eta_2 \frac{4n+3}{n} C_n - 2[\eta](2n+1)(2n+3) P_{2n}(0) \left\{ (2n+1) D_n + (2n+2) D_{n+1} \right\}. \tag{28}$$

The two constants, $[p_0]$ and ζ_0, which appear in the solution, are determined by Eqs. (24) and (25). A simple calculation leads to

$$\zeta = Ca_{12} \sum_{n=1}^{\infty} \frac{Z_n}{(2n+2)^2} \left(2\frac{n+1}{n+2} r^2 - \frac{n}{n+2} - r^{2n+2} \right).$$

The shapes of the interface for $\eta = 1$ are demonstrated in Fig. 8(a); the deformations shown in this figure are typical within the whole range of $\eta_{1,2}$. The maximum deflection (the interface is distorted in the direction of the first liquid) occurs at the center $r = 0$ and the minimum one (the distortion is in the direction of the second liquid) takes place at a certain $r = r_m$. This structure of the interface deformation can be expected from the Hadamard–Rybczynski flow; indeed, near the drop surface the ϑ-component of the velocity is positive and therefore $\zeta < 0$ near the triple line. In contrast, at the center of the drop, the flow has the opposite direction and ζ is positive there.

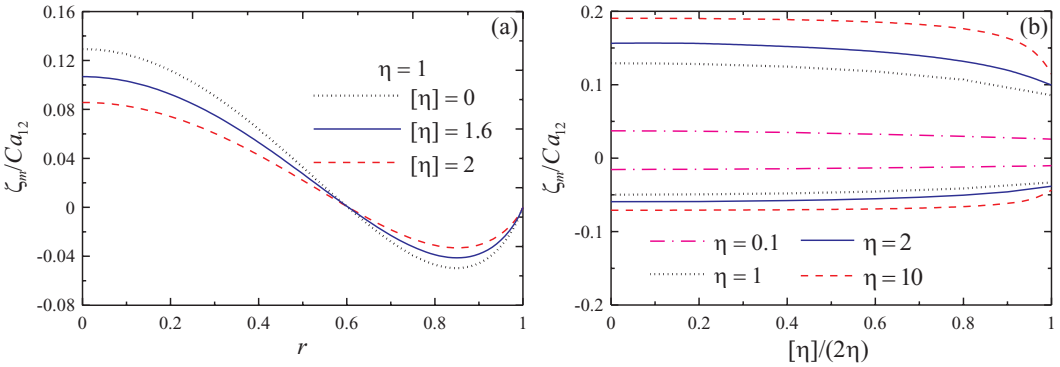

FIG. 8. Deformation of the internal interface by the flow. (a) Profiles $\zeta(r)$ at $\eta = (\eta_1 + \eta_2)/2 = 1$ and $[\eta] = \eta_2 - \eta_1 = 0$, 1.6, and 2 (dotted, solid, and dashed lines, respectively). (b) Variation of the maximum and minimum values of ζ with $[\eta]/(2\eta)$ for different η.

Although the internal interface changes the Hadamard–Rybczynski flow in the way discussed in Sec. III, the interface deformation still follows this flow.

Variation of the maximum and minimum values of the interface distortion is shown in Fig. 8(b). With increase in η the deformation becomes larger, but this effect is caused by nondimensionalization only. Indeed, a more appropriate way of introducing capillary number, which characterizes the deformation of the internal interface, is the scaling of $\tilde{\gamma}_{12}$ with the internal viscosities, for example, $(\tilde{\eta}_1 + \tilde{\eta}_2)U/\tilde{\gamma}_{12} = 2Ca_{12}\eta$. It means that the deformation at fixed $2Ca_{12}\eta$ is larger for smaller η and it is more pronounced for a less viscous drop, as one intuitively expects.

Increasing the viscosity contrast $[\eta]$ at fixed η, one can readily see the decrease in the interface deformation. Indeed, with growth of $[\eta]$, the typical flow velocity in the first liquid v_1 grows, whereas v_2 decays. In spite of the flow intensification, the pressure difference proportional to $\eta_2 v_2 - \eta_1 v_1$ shrinks, which makes the deformation smaller.

VI. CONCLUDING REMARKS

The motion of a Janus drop in an external uniform flow is addressed. Starting with the equilibrium configuration, we first find the shape of a nearly Janus drop in the absence of the flow. To that end the limiting case of small $[\gamma] = (\tilde{\gamma}_{02} - \tilde{\gamma}_{01})/\tilde{\gamma}_{12}$ and $\gamma^{-1} = 2\tilde{\gamma}_{12}/(\tilde{\gamma}_{01} + \tilde{\gamma}_{02})$ is analyzed. The former condition means that the difference of the surface tensions at the drop surface is small in comparison with the surface tension at the internal interface $\tilde{\gamma}_{12}$. The latter condition means that $\tilde{\gamma}_{12}$ is small with respect to the surface tension at the drop surface. Under these conditions both internal fluids occupy almost hemispherical domains.

Then, the Stokes flow past the perfect Janus drop is studied. At a small capillary number, the interfaces are assumed nondeformable due to the flow. Two generic cases, when the internal interface is (i) perpendicular to the external flow ($\beta = 0$, axisymmetric flow) and (ii) parallel to the flow ($\beta = \pi/2$, three-dimensional problem), are analyzed. It is shown that for any other value of β the velocity field can be represented as a superposition of the two above-mentioned solutions.

For $\beta = 0$ the vector potential of the velocity is introduced; it is presented by Eqs. (10) and (11) with the coefficients determined numerically. It is important that even for the equal internal viscosities, the problem is not reduced to the Hadamard–Rybczynski solution.[17,18] Indeed, the internal interface, with zero normal velocity there, provides an additional hindrance. Therefore, as shown in Fig. 3(a) the total force imposed on the Janus drop is larger than that for a single-fluid drop but less than for a solid sphere.

A small distortion of the internal interface is also found for this particular configuration. (The deformation of the drop surface is less by the factor γ^{-1}.) The interface follows the Hadamard–Rybczynski flow, the deflection is directed to the first (less viscous) liquid in the center and to the second (more viscous) liquid near the triple line.

For $\beta \neq 0$, the Lamb expansion of the velocity is used, see Eq. (14) and Appendix A. In this case, there also appears a torque {see Fig. 6(a)}, which tries to turn the freely rotating drop in such a way that $\beta = 0$. The stable configuration corresponds to the less viscous fluid situated at the upstream face of the drop.

We also confirm the results of analytical method by direct numerical computations for rather small Reynolds number, ANSYS Fluent is used to that end. This numerical approach can be applied to relax some of the model restrictions, such as hemispherical domains occupied by the internal fluids. In fact, we do not expect qualitative difference in the dynamics of such a realistic Janus drop. However, some important aspects needed for the experiments and/or technologies (such as the stable configuration, intensity of the flow inside the Janus drop, etc.) can be computed.

In contrast to a single-fluid drop, for a Janus one the imposed torque and the angular velocity of drop rotation can be coupled. Indeed, the Janus drop has an additional internal interface, where the normal velocity can be prescribed which corresponds to the drop rotation around the axis belonging to the internal interface. On the other hand, if the torque is normal to the internal interface, the Janus drop is similar to the single-fluid one. Therefore, a Janus particle is an object intermediate between a simple drop and a solid particle, for which the "external forcing" (the velocity, angular velocity, and shear rate of the ambient far from the particle) and the "response" (force, torque, and stress applied

to the particle) are coupled via the mobility tensor. From practical point of view, it is important to study a Janus drop behavior under a uniform shear. We expect that the dynamics of a Janus drop under this condition has a certain similarity to the stick-slip sphere.[14,15,34] The generic feature is that the spherical body with a broken fore-and-aft symmetry behaves in an external flow like a spheroid or other body of revolution; hence, dynamics similar to that found in Ref. 35 is expected.

We have completely disregarded mixing processes in the analysis, which can be important in view of large contrast in the surface tensions, the surface tension at the internal interface, $\tilde{\gamma}_{12}$, is smaller than the others, $\tilde{\gamma}_{01}$ and $\tilde{\gamma}_{02}$. On the one hand, generally speaking, small surface tension does not necessarily result in mixing; if the liquids have complex and different structures of molecules, the pair of internal fluids still can be immiscible. On the other hand, the flow inside the drop is shown to be of small intensity, especially near the internal interface, where the stagnant zone develops. Hence, the role of advection in a mixing is negligible, whereas another candidate, the molecular diffusion, is rather small. The typical value of the Schmidt number, the ratio of the characteristic times of mass and momentum diffusion, is at least about 100 for most of the liquid mixtures. Therefore, having been created, Janus drop has enough time to relax the momentum and, consequently, approach the stable state, before the mixing produces a valuable effect. Thus, the mixing in a forced Janus drop has to be studied only for the stable configuration.

ACKNOWLEDGMENTS

We are grateful to N. A. Rukavishnikova and D. S. Goldobin for fruitful comments. This publication is based on work supported by Award No. RUP1-7078-PE-12 (joint grant with Ural Branch of the Russian Academy of Sciences) of the U.S. Civilian Research & Development Foundation (CRDF Global) and by the National Science Foundation under Cooperative Agreement No. OISE-9531011. This work was partly supported by the National Science Foundation; CAREER Award (CBET-1055284).

APPENDIX A: REPRESENTATION OF THREE-DIMENSIONAL VELOCITY FIELDS FOR $\beta = \pi/2$

For $\beta = \pi/2$, we represent the harmonic functions χ, $\bar{p}$, and Φ in the surrounding fluid as follows:

$$\chi^{(0)} = \sum_{n=1}^{\infty} H_n r^{-n-1} P_n^{(1)}(\theta) \sin\phi, \tag{A1a}$$

$$\bar{p}^{(0)} = \sum_{n=1}^{\infty} \frac{2(2n-1)}{n+1} E_n r^{-n-1} P_n^{(1)}(\theta) \cos\phi, \tag{A1b}$$

$$\Phi^{(0)} = \sum_{n=1}^{\infty} \frac{E_n}{n+1} r^{-n-1} P_n^{(1)}(\theta) \cos\phi. \tag{A1c}$$

This leads to the following expression for the velocity of this fluid:

$$v_r^{(0)} = \sum_{n=1}^{\infty} E_n P_n^{(1)}(\theta)(r^2-1) r^{-n-2} \cos\phi - L(r) \sin\vartheta \cos\phi, \tag{A2a}$$

$$v_\vartheta^{(0)} = \sum_{n=1}^{\infty} \left\{ \frac{E_n Q_n(\theta)}{n+1} \left(\frac{n-2}{n} r^2 - 1 \right) + H_n P_n'(\theta) r \right\} r^{-n-2} \cos\phi - M(r)\theta \cos\phi, \tag{A2b}$$

$$v_\phi^{(0)} = \sum_{n=1}^{\infty} \left\{ \frac{E_n P_n'(\theta)}{n+1} \left(\frac{n-2}{n} r^2 - 1 \right) + H_n Q_n(\theta) r \right\} r^{-n-2} \sin\phi + M(r) \sin\phi. \tag{A2c}$$

Inside the drop the Lamb functions are the following:

$$\chi^{(1,2)} = \left\{ \sum_{n=1}^{\infty} A_n^{(1,2)} r^{2n} P_{2n}^{(1)}(\theta) + \eta_{2,1} \sum_{n=0}^{\infty} G_n r^{2n+1} \frac{P_{2n+1}^{(1)}(\theta)}{P'_{2n+1}(0)} \right\} \sin\phi, \tag{A3a}$$

$$\begin{aligned} \bar{p}^{(1,2)} = & \sum_{n=0}^{\infty} B_n^{(1,2)} \frac{2(4n+5)}{2n+1} r^{2n+1} \frac{P_{2n+1}^{(1)}(\theta)}{P_{2n+1}^{(1)}(0)} \cos\phi \\ & + \eta_{2,1} \sum_{n=1}^{\infty} D_n \frac{2(2n+1)(4n+3)}{2n+3} r^{2n} \frac{P_{2n}^{(1)}(\theta)}{Q_{2n}(0)} \cos\phi, \end{aligned} \tag{A3b}$$

$$\begin{aligned} \Phi^{(1,2)} = & -\left\{ \sum_{n=0}^{\infty} \frac{B_n^{(1,2)}}{2n+3} r^{2n+3} \frac{P_{2n+3}^{(1)}(\theta)}{P_{2n+3}^{(1)}(0)} + \eta_{2,1} \sum_{n=1}^{\infty} D_n r^{2n+2} \frac{P_{2n+2}^{(1)}(\theta)}{Q_{2n+2}(0)} \right\} \cos\phi \\ & + \left\{ \sum_{n=0}^{\infty} F_n r^{2n+1} P_{2n}^{(1)} + \eta_{2,1} \sum_{n=0}^{\infty} G_n r^{2n+2} \frac{P_{2n+2}^{(1)}}{Q_{2n+2}(0)} \right\} \cos\phi. \end{aligned} \tag{A3c}$$

Therefore, the velocity fields can be written as

$$\begin{aligned} v_r^{(1,2)} = & \sum_{n=0}^{\infty} \left(B_n^{(1,2)} \left\{ \frac{P_{2n+1}^{(1)}(\theta)}{P_{2n+1}^{(1)}(0)} - \frac{P_{2n+3}^{(1)}(\theta)}{P_{2n+3}^{(1)}(0)} \right\} r^2 + (2n+1) F_n P_{2n+1}^{(1)}(\theta) \right. \\ & \left. + \eta_{2,1}(2n+2) G_n \frac{P_{2n+2}^{(1)}(\theta)}{Q_{2n+2}(0)} r \right) r^{2n} \cos\phi \\ & + \eta_{2,1} \sum_{n=1}^{\infty} D_n \left\{ \frac{2n(2n+1)}{2n+3} \frac{P_{2n}^{(1)}(\theta)}{Q_{2n}(0)} - (2n+2) \frac{P_{2n+2}^{(1)}(\theta)}{Q_{2n+2}(0)} \right\} r^{2n+1} \cos\phi, \end{aligned} \tag{A4a}$$

$$\begin{aligned} v_\vartheta^{(1,2)} = & -\sum_{n=0}^{\infty} \left(B_n^{(1,2)} \left\{ \frac{n+2}{(2n+1)(n+1)} \frac{Q_{2n+1}(\theta)}{P_{2n+1}^{(1)}(0)} - \frac{1}{2n+3} \frac{Q_{2n+3}(\theta)}{P_{2n+3}^{(1)}(0)} \right\} r^2 + F_n Q_{2n+1}(\theta) \right. \\ & \left. - \eta_{2,1} G_n \left\{ \frac{P'_{2n+1}(\theta)}{P'_{2n+1}(0)} - \frac{Q_{2n+2}(\theta)}{Q_{2n+2}(0)} \right\} r \right) r^{2n} \cos\phi \\ & + \sum_{n=1}^{\infty} \left(A_n^{(1,2)} P'_{2n}(\theta) - \eta_{2,1} D_n \left\{ \frac{Q_{2n}(\theta)}{Q_{2n}(0)} - \frac{Q_{2n+2}(\theta)}{Q_{2n+2}(0)} \right\} r \right) r^{2n} \cos\phi, \end{aligned} \tag{A4b}$$

$$\begin{aligned} v_\phi^{(1,2)} = & -\sum_{n=0}^{\infty} \left(B_n^{(1,2)} \left\{ \frac{n+2}{(2n+1)(n+1)} \frac{P'_{2n+1}(\theta)}{P_{2n+1}^{(1)}(0)} - \frac{1}{2n+3} \frac{P'_{2n+3}(\theta)}{P_{2n+3}^{(1)}(0)} \right\} r^2 + F_n P'_{2n+1}(\theta) \right. \\ & \left. - \eta_{2,1} G_n \left\{ \frac{Q_{2n+1}(\theta)}{P'_{2n+1}(0)} - \frac{P'_{2n+2}(\theta)}{Q_{2n+2}(0)} \right\} r \right) r^{2n} \sin\phi \\ & + \sum_{n=1}^{\infty} \left(A_n^{(1,2)} Q_{2n}(\theta) - \eta_{2,1} D_n \left\{ \frac{P'_{2n}(\theta)}{Q_{2n}(0)} - \frac{P'_{2n+2}(\theta)}{Q_{2n+2}(0)} \right\} r \right) r^{2n} \sin\phi. \end{aligned} \tag{A4c}$$

Here again $Q_n = \theta P'_n - n(n+1)P_n$.

These representations of velocity fields automatically satisfy the Stokes equation and boundary conditions at the internal interface, if

$$[B_n] = \frac{(n+1)(2n+1)^2(2n+3)^2}{4n+5} P_{2n}(0)[A_{n+1}],$$

where $[B_n] = B_n^{(2)} - B_n^{(1)}$. In addition, $v_r^{(0)}$ vanishes at $r = 1$.

Substituting this ansatz into remaining boundary conditions at $r = 1$ and projecting these conditions on $P_n^{(1)}$, one obtains the set of linear equations for the coefficients $A_n^{(1,2)}$, $B_n^{(1,2)}$, D_n, E_n, F_n, G_n, and H_n. This set of equations is solved numerically.

It should be emphasized that the convergence of the series is rather slow because of the presence of jump in the viscosities at $\vartheta = \pi/2$. In order to improve the convergence and to suppress the oscillations of the coefficients for large n, these harmonics have to be considered separately. Such an analysis results in the following asymptotics valid at large n:

$$A_n^{(1,2)} \sim (-1)^n n^{-7/2}, [A_n^{(1)}] \sim (-1)^n n^{-13/2}, B_n^{(1,2)} \sim n^{-2}, [B_n^{(1)}] \sim n^{-3}, \tag{A5a}$$

$$D_n \sim n^{-2}, F_n \sim (-1)^n n^{-9/2}, G_n \sim n^{-3}, \tag{A5b}$$

$$(E_{2n}, E_{2n+1}) \sim (-1)^n n^{-5/2}, (H_{2n}, H_{2n+1}) \sim (-1)^n n^{-5/2}, \tag{A5c}$$

where according to notations accepted in the paper $[A_n] = A_n^{(2)} - A_n^{(1)}$. These asymptotics must be taken into account when the series are cut; for instance, one can set $H_{2N+1} \approx -H_{2N-1}$ instead of simple vanishing H_{2n+1} at $n \geq N$. This procedure improves the convergence to a great extent.

The total force exerted on the drop (in the same units, $\tilde{\eta}_0 aU$) can be expressed as follows:

$$F_x = 2\pi(3 - E_1), F_z = 0, \tag{A6}$$

whereas for the y-component of the torque one obtains

$$T_y = -8\pi H_1. \tag{A7}$$

APPENDIX B: SIMPLIFICATION OF THE VELOCITY FIELDS FOR $\beta = \pi/2$ AT SMALL $[\eta]/\eta$

Let us briefly discuss the simplification of the general solutions given in Appendix A at small $[\eta]/\eta$. At the zeroth order with respect to this ratio the solution is given by Eq. (17), which corresponds to $F_0 = -E_1 = \mp B_0^{(1,2)} = \mu$, $F_1 = 2\mu/9$ in Eqs. (A2) and (A4), whereas the rest of the coefficients vanish.

The solution $\mathbf{u}^{(j)}$ at the first order is provided by the same formulas, Eqs. (A2) and (A4), with the symmetry properties following from Eq. (19):

$$F_n = E_{2n+1} = H_{2n} = 0, A_n^{(1)} = -A_n^{(2)} = A_n, B_n^{(1)} = -B_n^{(2)} = B_n.$$

In particular, from $E_1 = 0$ and Eq. (A6) one can conclude that the first correction to the velocity field $\mathbf{u}^{(j)}$ does not provide a correction to the force imposed onto the drop.

As one can see, the representation of the velocity corrections $\mathbf{u}^{(j)}$ contains half of the coefficients appearing in the general case. Indeed, one can satisfy the boundary conditions at $r = 1$ only for $\vartheta \leq \pi/2$, the boundary conditions for $\vartheta > \pi/2$ are met automatically due to the symmetry condition, Eq. (19).

Again, at large n the problem has to be analyzed separately in order to improve the convergence of the series. This provides

$$A_n \sim n^{-13/2}, B_n \sim n^{-3}, D_n \sim n^{-2}, G_n \sim n^{-3}, E_{2n} \sim (-1)^n n^{-5/2}, H_{2n+1} \sim (-1)^n n^{-7/2},$$

which is closely related to Eq. (A5).

[1] P. G. de Gennes, "Soft matter," Rev. Mod. Phys. **64**, 645 (1992).
[2] F. Wurm and A. F. M. Kilbinger, "Polymeric Janus particles," Angew. Chem. Int. Ed. **48**, 8412 (2009).

[3] J. Yoon, K. J. Lee, and J. Lahann, "Multifunctional polymer particles with distinct compartments," J. Mater. Chem. **21**, 8502 (2011).
[4] Z. Nie, W. Li, M. Seo, S. Xu, and E. Kumacheva, "Janus and ternary particles generated by microfluidic synthesis: design, synthesis, and self-assembly," J. Am. Chem. Soc. **128**, 9408 (2006).
[5] C.-H. Chen, R. K. Shah, A. R. Abate, and D. A. Weitz, "Janus particles templated from double emulsion droplets generated using microfluidics," Langmuir **25**, 4320 (2009).
[6] D. Dendukuri and P. S. Doyle, "The synthesis and assembly of polymeric microparticles using microfluidics," Adv. Mater. **21**, 4071 (2009).
[7] H. Hasinovic, S. E. Friberg, and G. Rong, "A one-step process to a Janus emulsion," J. Colloid Interface Sci. **354**, 424 (2011).
[8] K.-H. Roh, D. C. Martin, and J. Lahann, "Triphasic nanocolloids," J. Am. Chem. Soc. **128**, 6796 (2006).
[9] E. Bormashenko, Ye. Bormashenko, R. Pogreb, and O. Gendelman, "Janus droplets: liquid marbles coated with dielectric/semiconductor particles," Langmuir **27**, 7 (2011).
[10] N. Virgilio and B. D. Favis, "Self-assembly of Janus composite droplets at the interface in quaternary immiscible polymer blends," Macromolecules **44**, 5850 (2011).
[11] J. Happel and H. Brenner, *Low Reynolds Number Hydrodynamics* (Prentice-Hall, Englewood Cliffs, NJ, 1965).
[12] S. Kim and S. J. Karrila, *Microhydrodynamics: Principles and Selected Applications* (Butterworth-Heinemann, Boston, 1991).
[13] H. Brenner, "The Stokes resistance of an arbitrary particle. Part V. Symbolic operator representation of intrinsic resistance," Chem. Eng. Sci. **21**, 97 (1966).
[14] J. W. Swan and A. S. Khair, "On the hydrodynamics of 'slip-stick' spheres," J. Fluid Mech. **606**, 115 (2008).
[15] G. Willmott, "Dynamics of a sphere with inhomogeneous slip boundary conditions in Stokes flow," Phys. Rev. E **77**, 055302(R) (2008).
[16] Y. Matunobu, "Motion of a drop suspended in a viscous flow with arbitrary velocity profile," J. Phys. Soc. Jpn. **29**, 508 (1970).
[17] J. S. Hadamard, "Mouvement permanent lent d'une sphere liquide et visqueuse dans un liquide visqueux," C. R. Acad. Sci. **152**, 1735 (1911).
[18] W. Rybczynski, "Über die fortschreitende Bewegung einer flüssigen Kugel in einem zähen medium," Bull. Acad. Sci. Cracovie 40 (1911).
[19] A. Acrivos, "The breakup of small drops and bubbles in shear flows," *Fourth International Conference on Physicochemical Hydrodynamics* [Ann. N.Y. Acad. Sci. **404**, 1 (1983)].
[20] J. M. Rallison, "The deformation of small viscous drops and bubbles in shear flows," Annu. Rev. Fluid Mech. **16**, 45–66 (1984).
[21] S. S. Sadhal and R. E. Johnson, "Stokes flow past bubbles and drops partially coated with thin films. Part 1. Stagnant cap of surfactant film—exact solution," J. Fluid Mech. **126**, 237 (1983).
[22] R. E. Johnson and S. S. Sadhal, "Stokes flow past bubbles and drops partially coated with thin films. Part 2. Thin films with internal circulation—a perturbation solution," J. Fluid Mech. **132**, 295 (1983).
[23] Y. H. Mori, "Configurations of gas-liquid two-phase bubbles in immiscible liquid media," Int. J. Multiphase Flow **4**, 383 (1978).
[24] E. Rushton and G. A. Davies, "Settling of encapsulated droplets at low Reynolds numbers," Int. J. Multiphase Flow **9**, 337 (1983).
[25] S. S. Sadhal and H. N. Oguz, "Stokes flow past compound multiphase drops: The case of completely engulfed drops/bubbles," J. Fluid Mech. **160**, 511 (1985).
[26] R. E. Johnson and S. S. Sadhal, "Fluid mechanics of compound multiphase drops and bubbles," Annu. Rev. Fluid Mech. **17**, 289 (1985).
[27] H. A. Stone and L. G. Leal, "Breakup of concentric double-emulsion droplets in linear flows," J. Fluid Mech. **211**, 123 (1990).
[28] J. Guzowski, P. M. Korczyk, S. Jakiela, and P. Garstecki, "The structure and stability of multiple micro-droplets," Soft Matter **8**, 7269 (2012).
[29] L. G. Leal, *Advanced Transport Phenomena* (Cambridge University Press, Cambridge, 2007).
[30] M. Abramowitz and I. Stegun, *Handbook of Mathematical Functions* (Dover, New York, 1972).
[31] L. E. Payne and W. H. Pell, "The Stokes flow problem for a class of axially symmetric bodies," J. Fluid Mech. **7**, 529–549 (1960).
[32] V. G. Levich, *Physicochemical Hydrodynamics* (Prentice-Hall, Englewood Cliffs, NJ, 1962).
[33] H. Hasinovic and S. E. Friberg, "Destabilization mechanisms in a triple emulsion with Janus drops," J. Colloid Interface Sci. **361**, 581 (2011).
[34] A. Ramachandran and A. Khair, "The dynamics and rheology of a dilute suspension of hydrodynamically Janus spheres in a linear flow," J. Fluid Mech. **633**, 233 (2009).
[35] G. B. Jeffery, "The motion of ellipsoidal particles immersed in a viscous fluid," Proc. R. Soc. London, Ser. A **102**, 161 (1922).